Int J Adv Manuf Technol (2018) 94:2043–2056
DOI 10.1007/s00170-017-1001-y

ORIGINAL ARTICLE

Model for the prediction of 3D surface topography and surface roughness in micro-milling Inconel 718

Xiaohong Lu[1] · Xiaochen Hu[1] · Zhenyuan Jia[1] · Mingyang Liu[1] · Song Gao[1] · Chenglin Qu[1] · Steven Y. Liang[2]

Received: 9 May 2017 / Accepted: 16 August 2017 / Published online: 4 September 2017

Abstract Nickel-based superalloy Inconel 718 retains high strength at high temperature, which meets the requirements of micro-parts in the fields of aerospace, energy, and power. However, Inconel 718 is a kind of difficult-to-machine material. During the micro-milling process, scale effect, multiple regenerative effect, and dynamic response all affect its surface roughness, causing the prediction of surface roughness of micro-milled parts difficult. To solve this problem, we study the predictive modeling of surface roughness of micro-milled Inconel 718. Based on the previously built instantaneous cutting thickness model, cutting force model, and the dynamic characteristics of micro-milling system, the authors establish a flexible deformation model of micro-milling cutter generated by cutting force. Since the machined surface is generated by duplicating the tool profile on the workpiece surface, and based on the actual cutting trajectory as well as flexible deformation of micro-milling cutter, the authors build the surface topography simulation model to predict surface roughness and conduct experiments to verify the accuracy of the model. The research realizes the prediction of surface roughness of micro-milled Inconel 718 parts and partially reveals the machining mechanism of micro-milling.

Keywords Micro-milling · Inconel 718 · Model · Surface roughness · Surface topography

✉ Xiaohong Lu
lxhdlut@dlut.edu.cn

[1] School of Mechanical Engineering, Dalian University of Technology, Dalian, Liaoning 116024, People's Republic of China

[2] The George W. Woodruff School of Mechanical Engineering, Georgia Institute of Technology, Atlanta, GA 30332-0405, USA

1 Introduction

Surface roughness affects the corrosion resistance, abrasion resistance, light reflection, thermal conductivity, and service life of a part. The direct measurement of surface roughness of a micro-milled part is not easy in general because the typical part size is always less than 1 mm. At present, studies of surface roughness normally involve experimental and simulation methods. Experimental method requires a large number of experimental data and is not economical. Furthermore, because the experimental data are collected under specific machine tools and cutters, the prediction model based on the data then cannot be applied to other situations. Simulation method is mainly based on the factors that influence the formation of surface topography, explores the machining mechanism, simulates the vibration of cutting force, dynamic responses of the system and the other factors in the cutting process, and establishes mathematical models of the position of the cutter tooth relative to the workpiece. By simulation of the machining surface topography, the surface roughness can be obtained and cutting parameters can be optimized; eventually, the processing quality is ensured. Compared with experimental method, simulation method is fairly cost-effective.

Many scholars have studied the surface topography simulation of macro-milling. Lee et al. [1] found that the vibration caused by the high speed of the spindle deteriorated the geometric accuracy of the machined surface, and then proposed an algorithm to simulate the machined surface. Omar et al. [2] built a generic and improved model to predict the 3D surface topography in side milling operation. The model incorporated the effects of tool runout, tool deflection, system dynamics, flank face wear, and the tool tilting on the surface roughness. Arizmendi et al. [3] presented a model for the prediction of surface topography in peripheral milling operation considering tool vibration during the cutting process. The tool

vibrations were transformed into equivalent polynomial equations and solved for discrete positions along the feed direction by applying a standard root finder. The model could predict the topography and roughness values. Montgomery and Altintas [4] presented an improved model of the milling process. The kinematics of the cutter and workpiece vibrations were modeled. They discretized the processing time and adopted a 3D array to record the positions of the discrete points on the different tool teeth at different time in the workpiece coordinate system. With continuous updating during the milling process, they got the workpiece surface Z-coordinate, then reconstructed the surface geometry topography in dynamic milling process. The surface topography simulation method of conventional milling provides reference for micro-milling surface topography simulation.

The minimum cutting thickness phenomenon makes the conventional milling simulation method impossible to be used in micro-milling surface topography simulation. Some scholars have tried to simulate the surface topography of micro-milling. Peng et al. [5] established a simulation algorithm of machining surface topography considering tool vibration. They defined the surface topography of micro-milling process in four aspects—surface texture formation, interval, height, and direction—and found that the processing parameters and methods affected the surface topography of the workpiece. Chen and Savage [6] found that parameters including spindle speed, feed rate, depth of cut, and vibration affected surface roughness. Based on the principle of tool profile duplication and considering the influences of tool interference and dynamic response on surface forming, Ding et al. [7] established an integrated surface topography simulation model for vibration-assisted micro-milling process. By analyzing the effect of residual height on surface topography of ultra-precision milling, Wei [8] used the residual height of the machined surface to study the surface topography of ultra-precision milling optical parts and established a prediction model for surface topography of ball-end milling. Li [9] simplified the micro-milling cutter into a stepped cantilever structure and used the principle of virtual displacement to establish the micro-cutter flexible deformation model, coupled the amount of flexible deformation of the cutter to the cycloidal trajectory of cutting edge and established a micro-milling surface topography model. Kouravand and Imani [10] considered the geometrical features of cutting edge, along with the concept of minimum chip thickness for constructing the micro-channel surface texture using kinematic rules and transformation operators. ACIS, a 3D B-rep geometric kernel, was used as a geometric engine for simulation of surface texture produced in the micro-milling process. Based on the concept of minimum cutting thickness, Ren [11] proposed a simulation model of the bottom surface geometry topography in micro-milling process and achieved 2D simulation of micro-milling groove surface topography and the calculation of surface roughness *Ra*. Li et al. [12] measured the vibration between the workpiece and the tool and obtained the 3D surface micro-topography considering the vibration. Luo et al. [13] integrated a dynamic cutting force model, regenerative vibration model, machining system response model, and tool profile model, and modeled the complex surface generation process. Matlab Simulink was used to interactively perform the simulation. The effects of machining variables and tool characteristics on the surface generation were investigated through simulations. Zhou [14] simulated the forming process of micro-nanometric cutting 3D surface topography, realized the 3D topography prediction, and conducted analysis on the cutting surface. By analyzing various linear and nonlinear factors in the cutting process, Duan [15] used Matlab to build an integrated dynamic simulation model to simulate the cutting process and establish the microscopic simulation of the surface topography according to the principle of blade shape duplication.

The micro-milling surface roughness simulation model so far has not taken the effects of multiple regeneration and elastic recovery of machined surface into account. Because the diameter of the micro-milling cutter is relatively small, the tool deformation cannot be ignored as in conventional machining. Based on the previously established instantaneous cutting thickness model, the cutting force model, and the dynamic response characteristics analyses of the micro-milling system, and considering the effect of multiple regeneration effect, the minimum cutting thickness, and the elastic recovery of the machined surface in the micro-milling process, we build the surface topography simulation model of micro-milling Inconel 718. The model is based on the principle of blade shape duplication, which obtains the micro-milling surface roughness value and reveals the formation mechanism of the micro-milling surface topography.

2 Dynamic characteristic analyses of micro-milling system

2.1 Instantaneous cutting thickness model

In micro-milling process, because of the elastic recovery phenomenon of the machined surface, elastic recovery layer existing in previous period will be cut by tooth in the next round. Calculation of instantaneous cutting thickness in micro-milling should consider the machined surface elastic recovery. In this paper, the assumptions about machined surface elastic recovery in micro-milling process are as follows: there exists a maximum elastic recovery amount $\delta_{\max}$, which is related to the workpiece material and the cutting tool. Usually, $\delta_{\max}$ is less than the minimum cutting thickness. When instantaneous cutting thickness is larger than the maximum elastic recovery thickness $\delta_{\max}$, machined surface elastic recovery amount is the maximum of elastic recovery

amount. When instantaneous cutting thickness is equal to or smaller than the maximum elastic recovery amount $\delta_{\max}$, machined surface elastic recovery amount is the instantaneous cutting thickness. The maximum elastic recovery amount calculated by the formula given by Shi [16] is as follows:

$$\begin{cases} \delta_{\max} = \dfrac{3\cdot\sigma_s}{4\cdot E}\cdot r_e\cdot\left[2\exp\left(\dfrac{H}{\sigma_s}-\dfrac{1}{2}\right)-1\right] & h > \delta_{\max} \\ \delta = h & h \le \delta_{\min} \end{cases} \tag{1}$$

where σ_s is the tensile strength of workpiece, E is the modulus of elasticity of workpiece, r_e is the radius of the cutting edge, and H is the hardness of workpiece. The maximum elastic recovery amount $\delta_{\max}$ defined by Eq. (1) is about 20% of the tool edge radius. The physical properties of Inconel 18 are listed in Table 1.

Based on axial infinitesimal, according to cutter tooth which is out of cutting or not in the previous period, the calculation of instantaneous cutting thickness can be divided into two cases: cutter tooth immerses in the workpiece; cutter tooth loses contact with the workpiece. The detailed analyses are in [17]. Eventually, the instantaneous cutting thickness in micro-milling process can be expressed by the following formula:

$$h(\phi_{jl}) = \left[f_t\sin\phi_{jl} + \left(v^0{}_{jl} - v_{jl}\right) + hpr_{jl}\right]g(\phi_{jl}) \tag{2}$$

where f_t is feed per tooth, the projections of vibration displacement of lth infinitesimal part on jth cutter tooth can be expressed as $v^0{}_{jl}$ and v_{jl} along the direction of cutting thickness, and $v^0{}_{jl}$ and v_{jl} are the projections in previous period and current period, respectively. $g(\phi_j)$ is unit step function. The function decides whether the tooth is cutting the material currently.

$$\begin{aligned} g(\phi_{jl}) &= 1, && \phi_{st} < \phi_{jl} < \phi_{ex} \\ g(\phi_{jl}) &= 0, && \phi_j < \phi_{st} \ \text{or} \ \phi_{jl} < \phi_{ex} \end{aligned} \tag{3}$$

Cutting thickness compensation is expressed as

$$\begin{cases} hpr_{jl} = \delta^0_{jl} & h^0(\phi_{jl}) > 0 \\ hpr_{jl} = f_t\sin(\phi_{jl}) + hpr^0_{jl} & h^0(\phi_{jl}) \le 0 \end{cases} \tag{4}$$

where hpr is the cutting thickness compensation of current tooth cutting period, hpr^0 is the cutting thickness compensation of last tooth cutting period, δ^0 is the machined surface elastic recovery of last tooth cutting period, and $h^0(\phi_{jl})$ is the instantaneous cutting thickness in last tooth cutting period on lth infinitesimal of jth cutter tooth.

2.2 Micro-milling force model in micro-milling Inconel 718

In micro-milling process, there are major differences between the processes dominated by shear effect and the one by plow effect with minimum cutting thickness as division line. It is inaccurate to describe micro-milling forces by the same cutting effect. Therefore, it is essential to establish micro-milling force prediction model dominated by shear effect and by plow effect separately. The force prediction model used in this paper was established by research group early [18].

After the axial discretization of teeth, infinitesimal micro-milling force prediction model dominated by shear effect is as follows:

$$\begin{cases} dF_r = \left(K_{rc}\cdot h + K_{rp}\cdot A_p\right)dw \\ dF_t = \left(K_{tc}\cdot h + K_{tp}\cdot A_p\right)dw \\ dF_a = \left(K_{ac}\cdot h + K_{ap}\cdot A_p\right)dw \end{cases} \quad h \ge h_{\min} \tag{5}$$

where dF_r, dF_t, and dF_a are radial, tangential, and axial infinitesimal micro-milling forces, respectively; the unit is N. K_{rc}, K_{tc}, and K_{ac} are radial, tangential, and axial shear coefficients, respectively; the unit is N/mm^2. h is instantaneous cutting thickness; the unit is mm. K_{rp}, K_{tp}, and K_{ap} are radial, tangential, and axial plow coefficients, respectively; the unit is N/mm^3. A_p is the contact area between flank face of the tool and workpiece surface, and its unit is mm^2. $h_{\min}$ is the minimum cutting thickness, and its value is 0.7 μm. dw is the cutting width of the infinitesimal; the unit is mm.

When actual cutting thickness is larger than the minimum cutting thickness, shear-dominant regime is the main material deformation form. Infinitesimal cutting model is shown as in Fig. 1.

In Fig. 1, δ is the elastic recovery of machined surface. Point S is intersection of the minimum cutting thickness and arc of cutting-edge, namely material separation stagnation. Plastic slipping deformation of material happens in area above point S, while material ironed by cutting-edge slips off flank surface in area below point S. α_S, which is the angle between the line connecting point S and arc center of cutting-edge and Y-axis, is expressed as Eq. (6):

$$\alpha_S = \cos^{-1}\left(\frac{r_e - t_{\min}}{r_e}\right) \tag{6}$$

Thereinto, r_e is the radius of the cutting edge. $t_{\min}$ is the minimum cutting thickness with unit of mm [18].

Shadow area A_p in Fig. 1 is plowing area between flank surface of tools and workpiece. According to geometrical relation, A_p is expressed as

$$A_p = A_{AOS} + A_{AOB} - A_{BOS} \tag{7}$$

Table 1 Physical properties of Inconel 718

Properties	Value	Properties	Value
Density (kg/m^3)	8470	Thermal conductivity(W/m K)	11.2
Hardness (HV)	450.1[a]	Yield stress (MPa)	1110
Modulus of elasticity (GPa)	206	Strain rate (%)	23.3
Poisson's ratio	0.3	Tensile strength (MPa)	965

[a] The hardness of nickel-based alloy used is measured by HVS-1000Z produced by Shanghai Precision Instrument Co., Ltd.

Thereinto, A_{AOS} is area of sector AOS, A_{AOB} is area of triangle AOB, and A_{BOS} is area of triangle BOS.

Area of sector AOS is

$$A_{AOS} \approx \frac{1}{2} r_e^2 (\alpha_S + \alpha_0) \tag{8}$$

Area of triangle $AOB$is

$$A_{AOB} = \frac{1}{2} r_e \cdot l_{AB} \tag{9}$$

$$l_{AB} = \frac{\delta - r_e(1-\cos\alpha_0)}{\sin\alpha_0} \tag{10}$$

Area of triangle BOS is

$$A_{BOS} = \frac{1}{2} r_e \cdot l_{BO} \cdot \sin(\alpha_S + \alpha_0 + \alpha_P) \tag{11}$$

$$l_{BO} = \sqrt{r_e^2 + {l_{AB}}^2} \tag{12}$$

$$\alpha_P = \tan^{-1}(l_{AB}/r_e) \tag{13}$$

Finally, the contact area A_p between flank surface and workpiece is expressed as

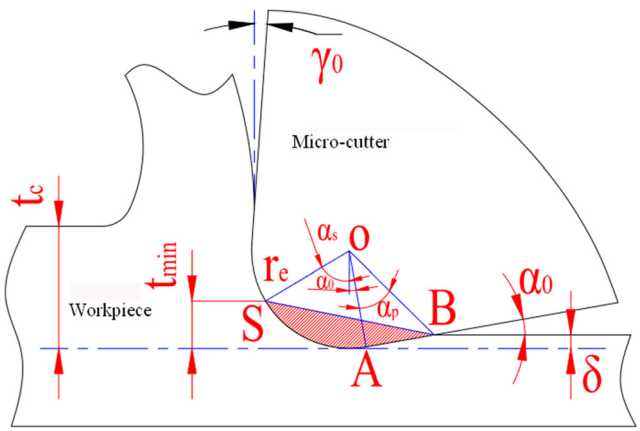

Fig. 1 Area of plowing processing

$$A_p = \frac{1}{2} r_e^2 (\alpha_S + \alpha_0) + \frac{1}{2} r_e \cdot l_{AB} - \frac{1}{2} r_e \cdot l_{BO} \cdot \sin(\alpha_S + \alpha_0 + \alpha_P) \tag{14}$$

Infinitesimal micro-milling force prediction model dominated by plowing effect is as follows:

$$\begin{cases} dF_r = (K_{rpp} \cdot A_p) dw \\ dF_t = (K_{cpp} \cdot A_p) dw \\ dF_a = (K_{app} \cdot A_p) dw \end{cases} \quad h < h_{\min} \tag{15}$$

where K_{rpp}, K_{cpp}, and K_{app} are radial, tangential, and axial plow coefficients, respectively; the unit of the three coefficients is N/mm^3.

When actual cutting thickness is smaller than the minimum cutting thickness, area A_p is as shown in Fig. 2. The maximum elastic recovery δ is regarded as a node to get plowing area in two situations.

As shown in Fig. 2a, when $\delta < t_c < t_{\min}$, it is supposed that elastic recovery of machined surface is the maximum elastic recovery. Calculation process of plowing area is similar to that of shear-dominant regime plowing area.

$$A_p = \frac{1}{2} r_e^2 (\alpha_C + \alpha_0) + \frac{1}{2} r_e \cdot l_{AB} - \frac{1}{2} r_e \cdot l_{BO} \cdot \sin(\alpha_C + \alpha_0 + \alpha_P) \tag{16}$$

Thereinto, $\alpha_C = \cos^{-1}\left(\frac{r_e - t_c}{r_e}\right)$ $l_{AB} = \frac{\delta - r_e(1-\cos\alpha_0)}{\sin\alpha_0}$ $l_{BO} = \sqrt{{r_e}^2 + {l_{AB}}^2}$ $\alpha_P = \tan^{-1}\left(\frac{l_{AB}}{r_e}\right)$.

As shown in Fig. 2b, when $t_c < \delta < t_{\min}$, it is supposed that elastic recovery of machined surface is complete elastic recovery. Elastic recovery is close to cutting thickness. Contact area is expressed as

$$A_p = \frac{1}{2} r_e^2 (\alpha_D + \alpha_0) + \frac{1}{2} r_e \cdot l_{AE} - \frac{1}{2} r_e \cdot l_{EO} \cdot \sin(\alpha_D + \alpha_0 + \alpha_{Pe}) \tag{17}$$

Thereinto, $\alpha_D = \cos^{-1}\left(\frac{r_e - t_c}{r_e}\right)$, $l_{AE} = \frac{t_c - r_e(1-\cos\alpha_0)}{\sin\alpha_0}$ $l_{EO} = \sqrt{{r_e}^2 + {l_{AE}}^2}$, $\alpha_{Pe} = \tan^{-1}\left(\frac{l_{AE}}{r_e}\right)$.

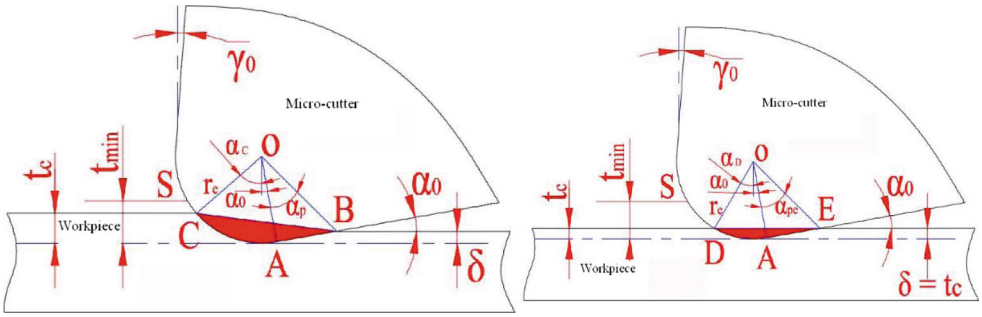

(a) δ< tc < tmin (b) tc<δ< tmin

Fig. 2 Area of plowing processing. **a** $\delta < t_c <$ tmin. **b** $t_c < \delta <$ tmin

The calculation of coefficients of Eqs. (5) and (15) was discussed in detail in the research of Lu et al. [18]. Coefficients of micro-milling force model are listed in Table 2.

2.3 Dynamic characteristic analysis of micro-milling system

Simplify the micro-milling dynamic system as two-degree-of-freedom model on orthogonal directions (X and Y directions), as shown in Fig. 3. It is assumed that there are N cutter teeth whose spiral angle is β, rotation direction of spindle is clockwise, angular velocity is Ω (rad/s), and feed direction of workpiece is negative direction of X-axis. The teeth are divided into M infinitesimal parts with a height of dz along the axial direction. The tooth position angle ϕ_{jl} of lth infinitesimal part on $j$thcutter tooth can be expressed as follows:

$$\phi_{jl} = \varphi - (j-1)\Phi_p - \frac{(l-1)\cdot dz\cdot \tan\beta}{R} \tag{18}$$

where φ is the tooth position angle of lth infinitesimal part on jth cutter tooth, R is the tool radius, Φ_p is the angle between two different teeth, and $\frac{(l-1)\cdot dz\cdot \tan\beta}{R}$ is the tooth position angle difference between current infinitesimal tooth and infinitesimal tooth at the end of the tool.

Micro-milling system is incented by micro-milling forces, which lead to the vibration of system. The vibration displacement is projected to X and Y directions. Then, the vibration displacement x and y are acquired on the orthogonal directions of the tool. The relationship between micro-milling forces and vibration displacement in the dynamic interaction of milling system is described according to the following dynamic equations:

$$\begin{cases} F_x(t) = \sum_{j=1}^{N}\sum_{l=1}^{M} F_{xjl} = m_x\ddot{x} + c_x\dot{x} + k_x x \\ F_y(t) = \sum_{j=1}^{N}\sum_{l=1}^{M} F_{yjl} = m_y\ddot{y} + c_y\dot{y} + k_y y \end{cases} \tag{19}$$

where m_x and m_y are quality factors of spindle-tool system on X and Y directions, respectively; c_x and c_y are damping coefficients of spindle-tool system on X and Y directions, respectively; k_x and k_y are rigidity coefficients of spindle-tool system on X and Y directions, respectively; N is the number of micro-milling cutter tooth; M is the total number of infinitesimal on tooth along the axial direction; and F_{xjl} and F_{yjl} are x and y components of the force on lth infinitesimal part of jth cutter tooth.

The calculation of dynamic character parameters of micro-milling system was discussed in [19]. Table 3 lists the dynamic character parameters of the micro-milling system.

Table 2 Coefficients of micro-milling force model on Inconel 718

Coefficients	Value	Coefficients	Value
K_{cc} (N/mm^2)	5.8181e3	K_{cp} (N/mm^3)	− 1.08258e6
K_{rc} (N/mm^2)	3.6715e3	K_{cpp} (N/mm^3)	3.3089e6
K_{ac} (N/mm^2)	7.3409e3	K_{rpp} (N/mm^3)	0.4669e6
K_{ap} (N/mm^3)	− 1.1202e6	K_{app} (N/mm^3)	4.5218e6
K_{rp} (N/mm^3)	− 0.6803e6		

3 The surface topography simulation of micro-milling process

3.1 The simulation principle of micro-milling process

The micro-milled surface is formed by the combination of several motions of the micro-milling cutter on the surface of the workpiece. The micro-milling cutter maps the tool profile on the workpiece surface along the actual cutting trajectory. From the geometric point of view, the machined surface is obtained by the Boolean subtraction operation of the micro-cutter geometrical profile along the actual cutting track and the workpiece surface, which means the machined surface topography is obtained by the principle of blade shape duplication.

In macro-machining, the schematic diagram of surface topography formation is shown in Fig. 4. The boundary point of the machined surface contour is determined by calculating the intersection of the two adjacent tool teeth profiles, and the cutting surface of the workpiece is obtained by connecting

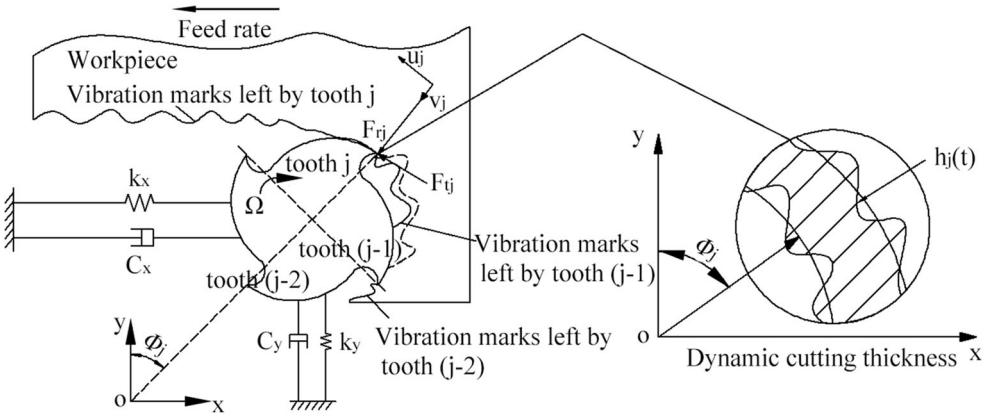

Fig. 3 Two-degree-of-freedom micro-milling system dynamic model

the two tool points. The tool profile relative to the workpiece is determined by the actual cutting trajectory of the tool during machining. The actual cutting trajectory of the tool is related not only to the cutting parameters but also to the dynamic characteristics of the machine-workpiece system during machining. In macro-machining, the dynamic relative displacement between tool and workpiece has little effect on the actual cutting trajectory of the tool due to the relatively large feed per tooth.

But in micro-milling process, the feed per tooth is very small and the tool teeth may run out while cutting or the subsequent tool marks may cut away the previous tool marks. As shown in Fig. 5, after the $i+1$th tool tooth finishes cutting, the $i+2$th tool tooth does not follow the ideal cutting track to finish cutting due to the influence of system vibration, etc. When the $i+3$th tooth is cutting, the tool marks of the tooth $i+2$th tooth is completely removed and it cannot affect the formation of surface topography. At this time, the surface topography is formed by the tool profile of $i+1$th tooth and $i+3$th tooth; this phenomenon is called tool cutting interference effect. The tool cutting interference effect is more common in precision machining where the feed is very small. The subsequent teeth will cut the higher residual surface cut by previous teeth due to the relative vibration between tool and workpiece. Therefore, in the micro-milling process, it is necessary to consider the influence of the tool cutting interference effect, calculate all intersecting tool profiles, and avoid just calculating the tool profiles within the intersection between two adjacent teeth so as not to cause micro-milling surface contour simulation distortion.

Table 3 Dynamic character parameters of the micro-milling system

	Modal mass (kg)	Rigidity (N/m)	Damping ratio
X direction	0.0048	1.455×10^6	0.0335
Y direction	0.0055	2.218×10^6	0.0311

3.2 Surface morphology simulation model considering the dynamic characteristics of micro-milling system

3.2.1 Milled surface topography model

Figure 6 shows the micro-milling process, where X is the feed direction, Y is the feed normal direction, and Z is the direction of the axis. The coordinate system is fixed on the workpiece, and the coordinate origin is the center point of the front end of the micro-milling cutter at an initial state.

It is known from tool movement that the tool does undergo some translations and simple harmonic movements along the X-axis and the Y-axis. The trajectory equation of the tip of the kth cutting edge in micro-milling process is obtained, which is shown as follows:

$$\begin{cases} X = ft + R\sin(wt - 2\pi k/K) \\ Y = R\cos(wt - 2\pi k/K) \\ Z = Z \end{cases} \tag{20}$$

where f is the feed rate, and the unit is μm/s; R is the tool diameter, and the unit is μm; w is the spindle speed, and the unit is rad/s; t is micro-milling processing time, and the unit is s; and K is the cutting edge number of micro-cutter.

This paper studies the sidewall surface topography during micro-end milling process. The rotating edge of the cutter is the helical line around the milling cutter cylinder. Helix angle

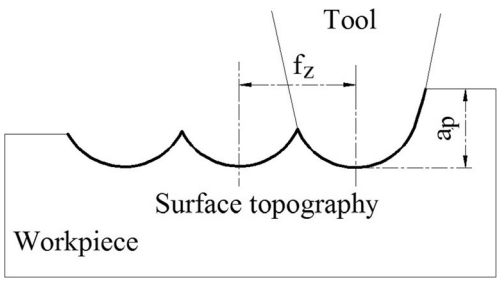

Fig. 4 Ideal surface produced by cutting

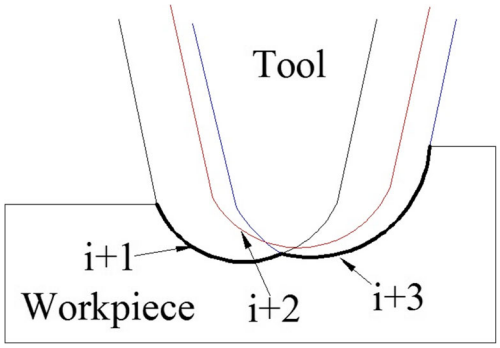

Fig. 5 Surface topography under the action of cutter interference

is β. According to Eq. (20), the ideal cutting trajectory of the Kth cutting edge of the micro-end mill with the helix angle β at the height Z is shown as follows:

$$\begin{cases} X = ft + R\sin(wt - 2\pi k/K - Z\tan(\beta)/R) \\ Y = R\cos(wt - 2\pi k/K - Z\tan(\beta)/R) \\ Z = Z \end{cases} \tag{21}$$

3.2.2 Flexible deformation model of micro-milling cutter

The diameter of the micro-milling cutter is between 0.1 and 1 mm. The stiffness of the cutter is relatively low. The cutting forces on the micro-cutter in micro-milling process cause the flexible deformation of micro-milling cutter. The flexible deformation of the tool changes the position of the profile duplication of the micro-milling tool on the machined surface of the part and changes the machined surface topography of the workpiece. At this point, the effect of the flexible deformation of the micro-milling cutter on surface topography cannot be ignored. When calculating the flexible deformation of the tool, the micro-cutter handle and the cutting edge are simplified to two cantilever structures, as shown in Fig. 7. A tool flexible

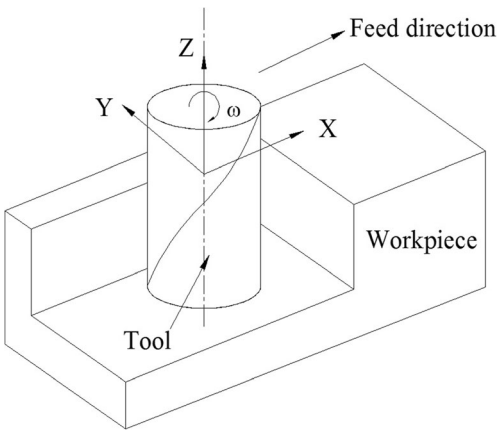

Fig. 6 Schematic drawing of micro-milling process

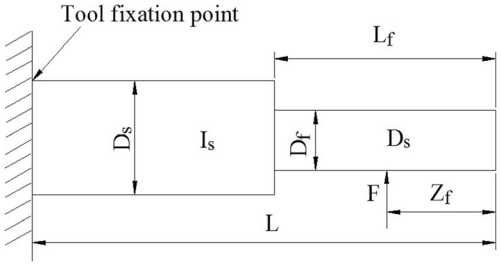

Fig. 7 Simplified model of micro-milling cutter

deformation model is established by a simplified micro-milling cutter in [13].

The micro-milling force acted on the cutting edge of the micro-milling cutter is equivalent to a concentrated force. The Z-coordinate of the point of action of the concentrated force is calculated as follows:

$$Z_f = L - \frac{\int_{\theta_s}^{\theta_e}(L-z)dF}{\int_{\theta_s}^{\theta_e}dF} = L - \frac{\int_{\theta_s}^{\theta_e}(L - r\theta/\tan\beta)dF}{\int_{\theta_s}^{\theta_e}dF} \tag{22}$$

where θ_s and θ_e are the angles of the instantaneously cut into and cut out. Z_f is the Z-coordinate of the equivalent concentrated force of the instantaneous cutting force in X direction and Y direction on the micro-cutter.$L$is the distance from the tool clamping part to the tip of the tool. According to the principle of virtual displacement, the tool flexible deformations in X and Y directions caused by the cutting force at the point of Z_f is as follows:

$$\begin{aligned} w_{(x,y)}(Z) = &-\frac{F_{(x,y)}}{6EI_f}\left[(Z_f - Z)^3 + 3(L_f - Z_f)^2(Z - L_f) + (L_f - Z_f)^3\right] \\ &-\frac{F_{(x,y)}}{6EI_s}\left[(L - Z_f)^2(3Z + 6L_f - 2L - Z_f) + (L_f - Z_f)^2(2L_f - 3Z + Z_f)\right] \end{aligned} \tag{23}$$

where $F_{(x,y)}$ is the cutting force of the tool in X and Y directions, E is the modulus of elasticity of the tool material, L_f is the length of the tool tooth, and I_f and I_s are the moment of inertia of the two stepped shafts which can be obtained by the following formula.

$$I_s = \frac{\pi}{64}D_s^4 \tag{24}$$

$$I_f = \frac{\pi}{64}(K_d D_f)^4 \tag{25}$$

where D_s is the diameter of the micro-cutter handle, D_f is the diameter of the micro-cutter teeth, and K_d is the equivalent diameter coefficient of the tool, which is set to 0.68.

3.2.3 Micro-milling surface morphology simulation model

When the cutting parameters and tool profile are determined, the machined surface topography in ideal machining condition can be obtained. In micro-milling process, due to the sharp decrease of the processing scale, the small diameter of the micro-milling cutter, the dynamic response characteristics of the micro-milling system, and the flexible deformation of the tool, the tool deviates from the ideal cutting trajectory, which affects the cutting surface topography. To better predict the micro-milling surface topography, based on the ideal surface topography modeling method, the previously built dynamic model of the micro-milling system and the flexible deformation model of micro-milling cutter, the authors build a simulation model of micro-milling surface topography.

The mathematical model of the real tool trajectory is shown in the following:

$$\begin{cases} X = ft + R\sin(wt - 2\pi k/K - Z\tan(\beta)/R) + x + w_x \\ Y = R\cos(wt - 2\pi k/K - Z\tan(\beta)/R) + y + w_y \\ Z = Z \end{cases} \quad (26)$$

where x and y are the dynamic displacements of the micro-cutter where the helix angle is β and the height is Z; the units are μm. w_x and w_y are the amount of flexible deformation of the cutter under the action of cutting force; the unit is μm.

By integrating the dynamic model of the micro-milling system, the flexible deformation model of the micro-milling cutter and the geometric model of the cutter profile, the micro-milling surface topography integration model is built. The flowchart is shown in Fig. 8. The input variables are the micro-milling parameters (spindle speed, feed per tooth, and cutting depth) and the geometry parameters of the micro-milling cutter. Based on the ideal cutting trajectory of the cutter, the instantaneous cutting thickness and instantaneous cutting force at this moment are calculated. According to the dynamic response model of the micro-milling system, the dynamic displacement of the cutter under the current cutting force is obtained, and added it into the ideal cutting trajectory of the cutter, and the actual cutting trajectory of the cutter is achieved.

At the same time, according to the physical and geometric characteristics of the cutter, the cutter deformations in x and y directions are solved under the instantaneous cutting force. Combined with the actual cutting tool trajectory and flexible deformation of the micro-milling cutter, the cutter profile is mapped to the workpiece surface based on the principle of blade shape duplication. After the extraction of the workpiece surface and the reconstruction of the surface topography of micro-milling side wall, the surface roughness is solved.

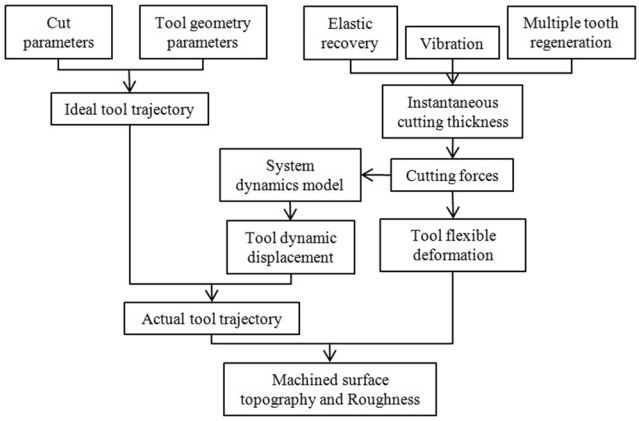

Fig. 8 Micro-milled surface topography model

3.3 Surface topography simulation algorithm

3.3.1 Extraction of micro-milled surface

(1) Nickel-based superalloy workpiece model

The feed per tooth of micro-milling is very small; due to the tool cutting interference effect, the machined surface topography in micro-milling process cannot be predicted correctly by locating the intersection points of geometric profile of the two adjacent teeth and calculating the trajectory of the micro-milling cutter between the intersection points. In this paper, the workpiece is dispersed. To obtain surface topography of micro-milling Inconel 718, the authors divided the workpiece into grids along the feed direction and axial direction. The authors then divided the length along feed direction and axial direction equally with the interval Δx and Δz and broke the entire workpiece into $m \times n$ small cubes. The process of micro-milling surface morphology formation is regarded as a process of continuous height updating of $m \times n$ small discrete cubes in geometric profile duplication of micro-milling cutter.

When the surface topography prediction model is built in the $m \times n$ grid points, the matrix $H = [h_{i,j}]$ ($i = 1, 2 \ldots, m$; $j = 1, 2, \ldots, n$) is used to represent the residual height of the corresponding position of the workpiece cutting surface. By searching each grid in turn, obtaining the residual height value, micro-milling surface topography is reconstructed. The simulation process is shown in Fig. 9. The meshing density should be set appropriately when meshing the workpiece. If the density of the mesh is too large, the tool element is too dense, resulting in a sharp increase in computation time or even failure. If the density of the mesh is too small, and every cell is too large, the surface topography simulation data distorts and cannot reflect the real cutting topography.

(2) Micro-unit of cutter setting

Micro-milling cutter is divided into micro-units, and the projected height of each axial micro-unit on the surface of

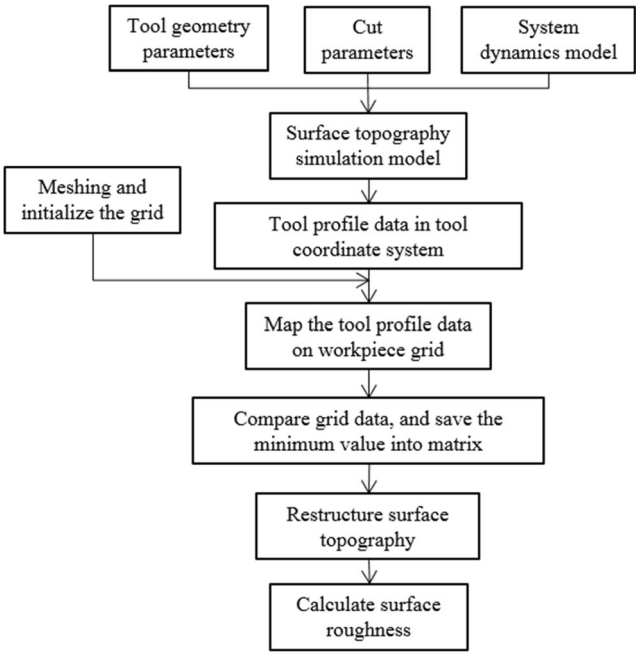

Fig. 9 The sketch map of the surface topography simulation

nickel-based superalloy workpiece is obtained. The length of the discrete units of the cutter is determined by the density of workpiece mesh generation. To ensure that after the workpiece mesh generation, each unit has geometric profile duplication of the cutter, that is, the micro-units that the tool tooth divided into can traverse all the workpiece grids. The projection length of the axial micro-units on the surface that have been meshed should be less than the minimum interval of the

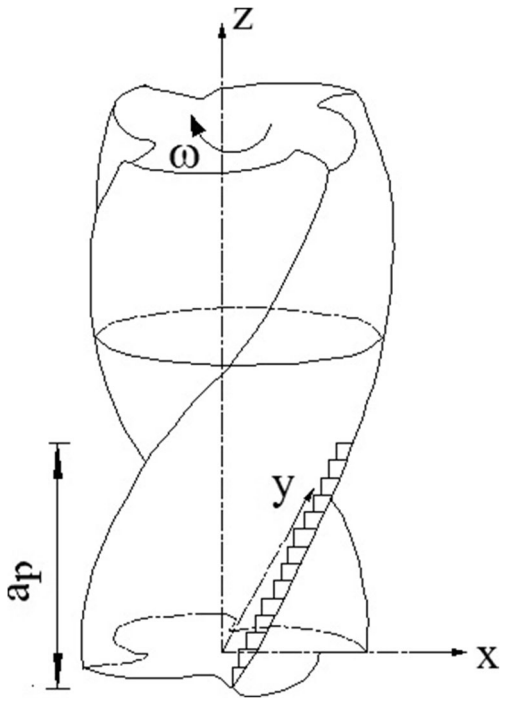

Fig. 10 Infinitesimal classification scheme of micro-milling cutter

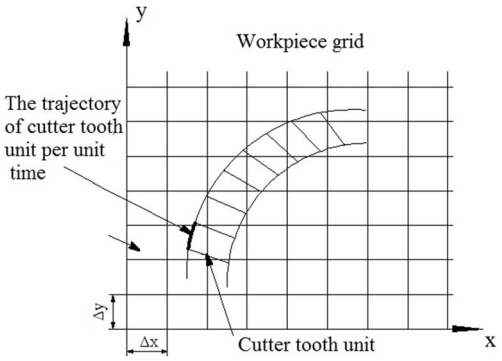

Fig. 11 Cutting trajectory projection drawing of blade infinitesimal

workpiece grid (as shown in Fig. 10). In the micro-milling process, micro-milling sidewall surface topography is affected by the part of the micro-milling cutter involved in the cutting. Therefore, only the cutting edge involved in cutting needs to be discretized in micro-units.

(3) Time step setting

To calculate the actual cutting trajectory of the micro-milling cutter teeth on Inconel 718 workpiece, except for the discretization of the axial micro-units of the tool teeth, it is also necessary to separate the processing time into multiple steps and calculate the cutting trajectory of each micro-unit of the tool in each unit time step (as shown in Fig. 11). In the micro-milling process, the tool moves in trochoid; the movement trajectory of the discrete point of the tooth is a trochoid. When setting the time step, it is necessary to ensure that the trochoid arc length in a unit time step is shorter than the workpiece grid length, that is,

$$\Delta s \leq \min(\Delta x, \Delta y) \tag{27}$$

where Δs is the arc length of trochoid movement in the unit step time, Δx is the length of the workpiece mesh generation along the feed direction, and Δy is the length of the workpiece mesh generation along the feed normal direction.

According to the trochoid formula, the calculation formula of the arc length per unit time is as follows:

$$ds = \sqrt{\left(\frac{dx}{dt}\right)^2 + \left(\frac{dy}{dt}\right)^2}\,dt = \sqrt{[f + Rw\cos(wt)]^2 + (Rw\sin wt)^2}\,dt \tag{28}$$

$$\Delta s = \int_0^{\Delta t} ds = \int_0^{\Delta t} \sqrt{[f + Rw\cos(wt)]^2 + (Rw\sin wt)^2}\,dt \tag{29}$$

where Δt is the unit step time. When the size of the workpiece mesh is determined, the maximum unit step time is then determined.

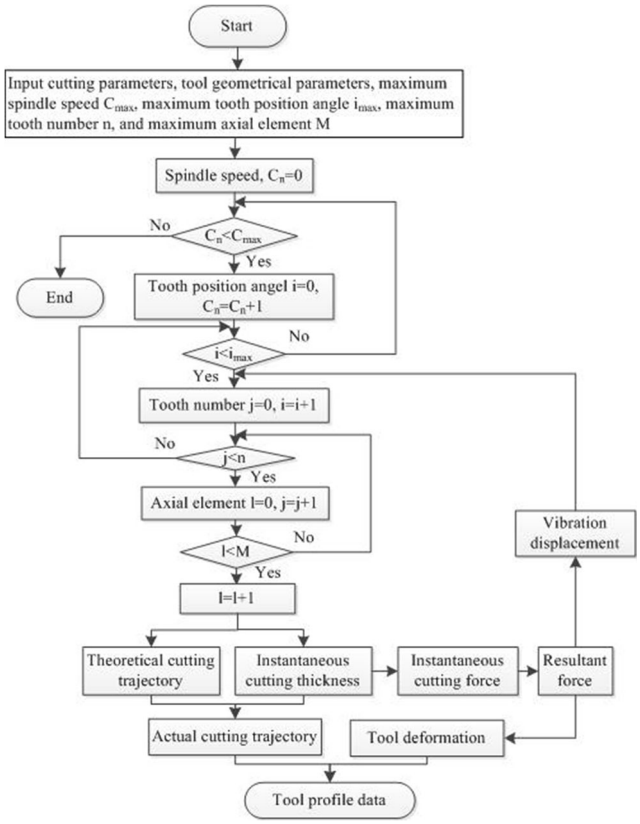

Fig. 12 The overall flowchart of the micro-milling surface topography simulation

3.3.2 Process of simulation program

Figure 12 describes the overall flowchart of the micro-milling surface topography simulation. The actual cutting trajectory of the tool is obtained by simulation of the micro-milling process. In Matlab program, a four-cycle nesting of the machining process will be done and the micro-milling process simulation is ultimately achieved.

(1) Rotation cycle of spindle.

In the micro-milling process, the spindle rotates at the specified spindle speed in the feed direction. After determining the micro-milling simulation time and the spindle speed, the number of spindle rotation in the simulation process is obtained. Set the spindle speed to S, with the unit of rpm, and set the total simulation time to T with the unit of second. Then, the number of spindle rotation in the micro-milling process is:

$$C = \left\lceil T \cdot S/60 - \frac{1}{2} \right\rceil \tag{30}$$

(2) The cycle of the tool tooth position.

After setting the time step, in each unit step time, the tool rotates by a certain angle, the angle of the tool tooth position, defined as the angle between the tool nose and the Y-axis of the workpiece coordinate system, changes. When the spindle rotates a full circle, the angle of the tool tooth position changes from 0 to 2π. If the tooth position angle is represented as ϕ, the tooth position angle at time t is calculated as follows:

$$\phi(t) = \Omega t \tag{31}$$

where Ω is the rotation angular velocity of the spindle; the unit is rad/s; Ω is determined by the spindle rotation speed. The relationship between them is as follows:

$$\Omega = \frac{2\pi \cdot S}{60} \tag{32}$$

When the time step and spindle speed are set, and spindle rotates a full circle, the times that the tool tooth position angle changes are calculated. Every rotation of the tool is regarded as a micro-unit. Then, $i_{\max}$ micro-units form when the spindle rotates a full circle. The instantaneous tooth position angle is $d\phi$ in a unit time step. The calculation relationship among the unit time step Δt, the instantaneous tooth position angle $d\phi$, and the micro-unit number $i_{\max}$ in a full-circle spindle rotation is as follows:

$$d\phi = \Omega \cdot \Delta t = \frac{2\pi \cdot S}{60} \Delta t \tag{33}$$

$$i\max = \frac{2\pi}{d\phi} \tag{34}$$

(3) The cycle of cutting edge conversion

Micro-milling cutters normally have more than one tool tooth, and common micro-milling cutters have two or four cutting edges. Therefore, at the same time, there are several cutting edges involved in cutting. At this point, the cutting force is the composition of cutting forces on each cutting edge involved in cutting. There is an angle between the cutter teeth, and the instantaneous tooth position angle of the different teeth in the micro-milling process is different at the same time. The angle Φ_p between N cutting edges tips is calculated as follows:

$$\Phi_p = 2\pi/N \tag{35}$$

The micro-milling cutter teeth are numbered according to the order when the tooth involves in cutting for the very first

Fig. 13 The system of micro-milling machine

time. The first tooth involved in cutting is the first tooth. The tooth position angle of the first tooth is ϕ at time t. Then, the tooth position angle of jth tooth at time t is calculated as follows:

$$\phi_j = \phi - (j-1)\Phi_p \tag{36}$$

(4) Cutting edge axial dispersion cycle

The cutting edge of micro-milling cutter has helix angle. Therefore, the instantaneous tooth position angle and instantaneous cutting thickness are varied at different heights at the same time. To simulate the actual micro-milling process, the micro-milling cutter is axially discretized to calculate the instantaneous tooth angle and instantaneous cutting thickness of each axial micro-units at the same time. The instantaneous cutting force of each axial micro-unit is calculated with the instantaneous cutting thickness, and the instantaneous cutting force of the micro-milling cutter is the composition of instantaneous cutting force of axial micro-units on each tooth.

$$M = \left\lceil \frac{ap}{dz} - \frac{1}{2} \right\rceil \tag{37}$$

Because the cutting edge of the micro-milling cutter has helix angle, there is a relationship between positions of axial micro-units on the micro-milling cutter. The first micro-unit on the tool nose is numbered first, and the instantaneous tooth position angle of the lth micro-unit on jth tooth is then calculated as follows:

$$\phi_{jl} = \phi - (j-1)\Phi_p - \frac{(l-1)\cdot dz\cdot \tan\beta}{R} \tag{38}$$

where β is the helix angle of the micro-milling cutter, R is the radius of the micro-milling cutter, and $\frac{(l-1)\cdot dz\cdot \tan\beta}{R}$ is the difference of the tooth position angle between the lth axial micro-unit and the first axial micro-unit caused by the helix angle of the micro-milling cutter. The micro-milling process is simulated by the four-cycle nesting above. The determination of the revolution of the spindle by the simulation time and the spindle speed is the outermost loop deciding whether the simulation continues, and the determination of the times that the tooth position angle changes, when the spindle rotates a full circle from the unit step and the spindle speed, as well as the calculation of the cutting state in turn at each tooth position angle, is the second loop of the simulation system. The changing times of the tooth angle when it reaches the maximum, that is, the micro-units number at the tooth position angle $i_{\max}$ is regarded as the judgment condition of whether to end the loop after the spindle completes one cycle of rotation. The multiple teeth involved in cutting at a certain tooth position angle when the spindle rotates a full circle is regarded as the third cycle.

The tooth position angle of each tooth at a certain time is calculated, and the maximum number of the teeth is regarded as the judgment condition of whether to end the third loop. The calculation of each axial micro-unit cutting state at the certain tooth position angle, the certain tooth number, and the certain revolution of the spindle is regarded as the fourth loop of the simulation. The instantaneous tooth position angle and instantaneous cutting thickness of each axial micro-unit as well as the instantaneous cutting force are calculated. The number of the axial micro-units is regarded as the judgment condition of whether to jump out the fourth loop. According to the loops above, the resultant force is solved by accumulating the cutting force of all tool micro-units at a certain teeth position angle in a certain lap of the spindle rotation. The displacement solved in the fourth loop is added to the machining

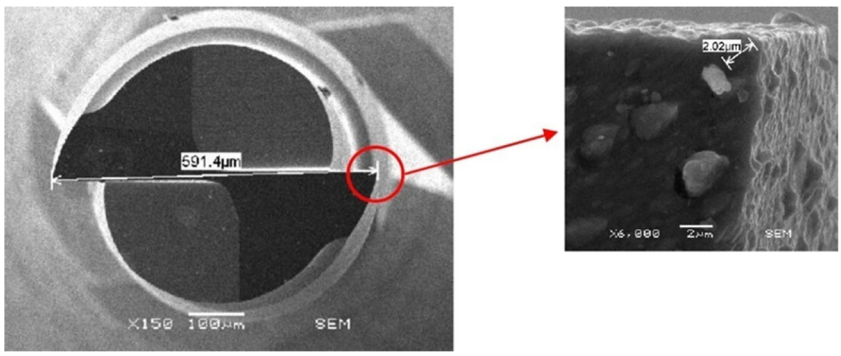

Fig. 14 The SEM photo of micro-milling tool's end

Table 4 Comparison between computational and experimental surface roughness

No.	Axial cutting depth $a_p/\mu m$	Spindle speed S/rpm	Feed per tooth $f_z/\mu m \cdot z^{-1}$	Simulation results	Experimental results	Relative error
1	55	40,000	0.5	0.38	0.42	10.5%
2	55	50,000	0.5	0.41	0.46	10.9%
3	55	60,000	0.5	0.29	0.32	9.4%
4	55	40,000	1.1	0.47	0.51	7.8%
5	55	50,000	1.1	0.40	0.41	2.4%
6	55	60,000	1.1	0.44	0.44	0.0%

simulation in the next moment. The machining position from the ideal cutting trajectory and vibration displacement at this moment are accumulated and set as the initial position in next cycle, and simulation program continues into next cycle.

3.3.3 Surface topography reconstruction in micro-milling process

The 3D coordinates of the actual cutting trajectory of the micro-milling cutter axial micro-unit at every moment are obtained by simulating the micro-milling process. The micro-milling surface morphology is obtained by the Boolean subtraction operation of the actual cutting trajectory of the axial micro-units and the surface of the workpiece. Therefore, it is necessary to extract the data from the coordinate point set of the actual cutting trajectory of all the micro-units that was obtained previously and to find the data points that eventually form the surface topography. The specific operation process of the program is as follows:

(1) Build the workpiece model, and mesh the part of the workpiece that has been machined. Create a matrix $H=[h_{i,j}]$ $(i=1,2\ldots,m;j=1,2,\ldots,n)$ based on the size of the grid and the area of the machined workpiece, where i is the number of workpiece micro-units in the feed direction and j is the number of the workpiece micro-units in the axial direction. Set the initial value to the matrix $H=[h_{i,j}]$ to represent the initial height of the workpiece.

(2) Correspond with the actual cutting trajectory coordinates obtained by each of the micro-element to specific moment (specific revolution, specific tooth position angle, specific position, specific tooth number, and specific axial micro-unit number). Run the nested loop introduced in Sect. 3.3.2 again. Search the actual cutting trajectory coordinates for each moment and each tool tooth micro-unit. Determine whether the cutting trajectory coordinates are in the machined area. If it is not in the machined area, the program proceeds to the next loop. If it is in the machined area, the program searches the corresponding position of the cutting trajectory coordinate value in the matrix $H=[h_{i,j}]$.

(3) Compare the height coordinate of the tool tooth discrete point at the moment with the height coordinate at the corresponding position in the matrix $H=[h_{i,j}]$. If the height of the tool tooth discrete point is smaller at the moment, it is proved that the micro-milling cutter cuts into the workpiece and the micro-milling cutter effects the formation of the workpiece surface topography. The data in the matrix $H=[h_{i,j}]$ is updated to the discrete point coordinates at this moment. Otherwise, the program keeps the original data.

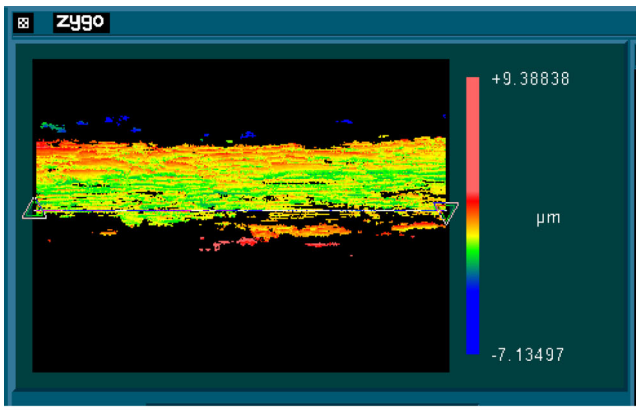

(a)The map of micro-milling topography

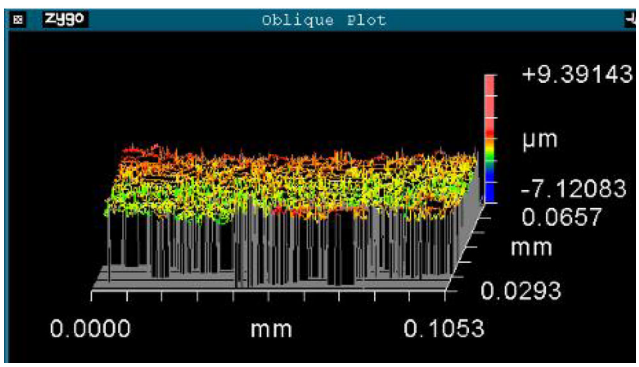

(b)The 3D topography of micro-milling

Fig. 15 Surface topography measurement of micro-milling by Zygo. **a** The map of micro-milling topography. **b** The 3D topography of micro-milling

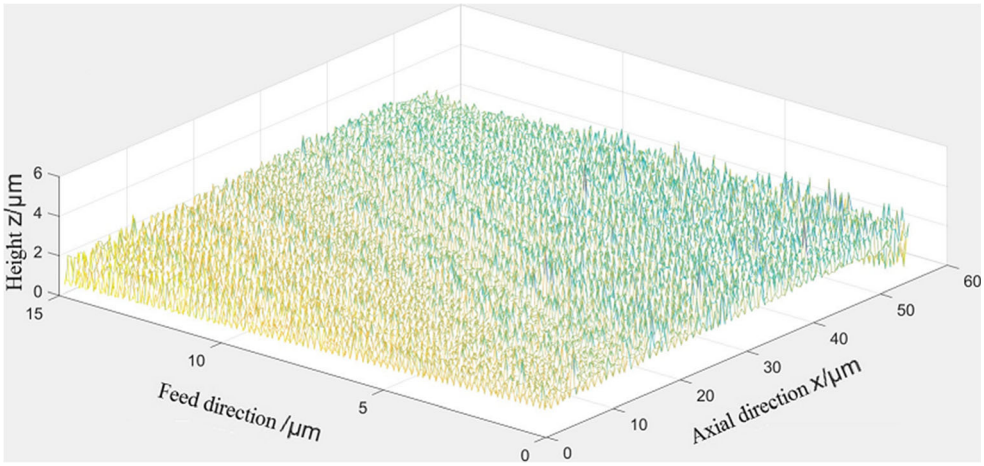

Fig. 16 Simulation chart with considering tool flexible deformation

(4) Determine whether all the coordinate points of the actual trajectory are in the machined area. Search for the corresponding position in the matrix $H = [h_{i,j}]$ and compare the coordinate value, extract the coordinate points of actual cutting trajectory. The data stored in matrix H is the data that constitute the micro-milling surface topography. Using the 3D graphic drawing command in Matlab, the surface topography of micro-milling can be drawn. Also, the data in matrix H are used as a source to study the characteristics of micro-milling surface features.

4 Surface topography simulation model validation

Micro-milling Inconel 718 experiments are conducted to validate the built surface roughness and topography model. Surface roughness (*Ra*) is measured under different combination of cutting parameters. The experimental results are compared with the output of the model to verify the accuracy of the established surface roughness prediction model.

4.1 Experimental and testing equipment

The experiments are carried out on the self-developed three-axis micro-milling machine (Fig. 13). The body size of the machine is 194 mm (X) × 194 mm (Y) × 400 mm (Z), and the workspace size is 50 mm (X) × 50 mm (Y) × 102 mm (Z). The feed system in X, Y, and Z directions use servo motor to drive precise ball screw. The feed system is equiped with linear encoders with absolute position accuracy of 1 μm and repeat position accuracy of 0.2 μm. The workpiece material is Inconel 718. The selected cutting tools are ultrafine particle-coated cemented carbide end-milling tools with two flutes whose diameter is 0.6 mm made by Union Tool Co. The actual diameter of the cutter is 594.1 μm tested by SEM (Fig. 14), the arc radius of cutting- edge is 2 μm, and the clearance angle is approximately 5°. The surface roughness values at the side wall of the milled slots are measured by the New View 5022 3D surface profiler produced by American Zygo Company.

4.2 Design of experiments

Experiments are designed to realize the micro-milling of micro-channels on Inconel 718. Surface roughness (*Ra*) and surface morphology under different combination of cutting parameters are measured to validate the built model. To make the results more reliable, the measurements are conducted three times for each cutting condition. The surface roughness value at three different positions of a groove is measured and the average value is taken as the final result of the experiment. Six groups of experiments are conducted. The simulation output compared with the experimental measurements are shown in Table 4.

Table 4 shows that the surface roughness of micro-milled surface is less than 1 μm, which achieves the submicron machining accuracy. The maximum relative error between computational and experimental surface roughness is 10.9%, and the average relative error is 6.8%. The comparison confirms that the established surface roughness predictive model can predict the micro-milled surface roughness.

Figure 15 shows the surface morphology measured by the New View 5022 3D surface profiler produced by American Zygo Company under one group cutting parameter (spindle speed is 50,000 rpm, feed per teeth is 0.5 μm, cutting depth is 55 μm). Figure 16 is the 3D morphology simulation results of the micro-milled Inconel 718 parts under the same cutting parameter. Comparing Fig. 15 with Fig. 16, we can find that from the nose of the cutter to the clamping part, the height of part's residule surface becomes large and the change trend is consistent, which means the built surface roughness and surface morphology model is effective.

5 Conclusions

To predict micro-milling surface roughness of Inconel 718, this paper combines the ideal cutting trajectory of micro-milling and system dynamic response model which considers the minimum cutting thickness, multiple regenerative effect, and elastic recovery to obtain actual cutting trajectory of micro-milling cutter. Considering that the machined surface is generated by duplicating the tool profile on the workpiece surface, and based on the flexible deformation of micro-milling cutter generated by cutting force, the simulation model of micro-milling surface topography is established. The simulation algorithm of 3D surface topography of micro-milling is compiled in Matlab. We take arithmetical mean deviation of the profile *Ra* as evaluation index of surface roughness and conduct micro-milling experiments to compare the simulation results with experimental values. The comparison shows that the maximal relative error is 10.9% and the average relative error is 6.8%. Moreover, we also compare surface topography from simulation and measurement, and the result shows that the built simulation model can predict surface topography. The research offers reference to predict micro-milling surface roughness of nickel-based superalloy and to reveal mechanism of micro-milling.

Acknowledgments The research is supported by the National Natural Science Foundation of China under Grant No. 51305061 and the State Foundation for Studying Abroad (CSC) under project number 201606065043. The financial contributions are gratefully acknowledged.

References

1. Lee KY, Kang MC, Jeong YH, Lee DW, Kim JS (2001) Simulation of surface roughness and profile in high-speed end milling. J Mater Process Technol 113(1):410–415
2. Omar OEEK, El-Wardany T, Ng E, Elbestawi MA (2007) An improved cutting force and surface topography prediction model in end milling. Int J Mach Tools Manuf 47(7):1263–1275
3. Arizmendi M, Campa FJ, Fernández J, de Lacalle LL, Gil A, Bilbao E, Lamikiz A (2009) Model for surface topography prediction in peripheral milling considering tool vibration. CIRP Ann Manuf Technol 58(1):93–96
4. Montgomery D, Altintas Y (1991) Mechanism of cutting force and surface generation in dynamic milling. J Eng Ind 113(2):160–168
5. Peng F, Wu J, Fang Z, Yuan S, Yan R, Bai Q (2013) Modeling and controlling of surface micro-topography feature in micro-ball-end milling. Int J Adv Manuf Technol 67(9–12):2657–2670
6. Chen JC, Savage M (2001) A fuzzy-net-based multilevel in-process surface roughness recognition system in milling operations. Int J Adv Manuf Technol 17(9):670–676
7. Ding H, Chen SJ, Cheng K (2011) Dynamic surface generation modeling of two-dimensional vibration-assisted micro-end-milling. Int J Adv Manuf Technol 53(9):1075–1079
8. Wei LF (2008) Surface topography prediction and simulation of optical parts in ultra-precision milling. Doctor Thesis. Dissertation, Huazhong University of Science and Technology. In Chinese
9. Li CF (2008) Study on force and surface topography modeling and process optimization of meso-scale end-milling. Doctor Thesis. Dissertation, Shanghai Jiao Tong University. In Chinese
10. Kouravand S, Imani BM (2014) Developing a surface roughness model for end-milling of Micro-Channel. Mach Sci Technol 18(2): 299–321
11. Ren CY (2008) Analysis on surface topography generation in micro-milling. Manuf Technol Mach Tool (1):36–39. In Chinese
12. Li RB, Zhang ZH, Li JG (2000) Prediction of 3D surface topography in ultra- precision machining. China Mech Eng 11(8):845–848 In Chinese
13. Luo XC, Cheng K, Ward R (2005) The effects of machining process variables and tooling characterization on the surface generation. Int J Adv Manuf Technol 25(11):1089–1097
14. Zhou L (2009) Dynamic micro/nano cutting system modeling for prediction and analysis of surface topography. Doctor Thesis. Dissertation, Harbin Institute of Technology. In Chinese
15. Duan YK (2006) The model and analysis of micro structure surface in ultra precision turning. Doctor Thesis. Dissertation, Harbin Institute of Technology. In Chinese
16. Shi WT (2011) Micro cutting technology. China Machine Press, Beijing In Chinese
17. Lu XH, Jia ZY, Wang FR, Li GJ, Si LK, Gao LS (2016) Model of the instantaneous undeformed chip thickness in micro-milling based on tooth trajectory. Proc Inst Mech Eng B J Eng Manuf. https://doi.org/10.1177/0954405416639890
18. Lu XH, Jia ZY, Wang XX, Li GJ, Ren ZJ (2015) Three-dimensional dynamic cutting forces prediction model during micro-milling nickel-based superalloy. Int J Adv Manuf Technol 81(9–12):2067–2086
19. Lu XH, Jia ZY, Wang H, Wang XX, Si LK, Gao LS (2016) Stability analysis for micro-milling nickel-based superalloy process. Int J Adv Manuf Technol 86(9–12):2503–2515